APPLICATIONS OF DIGITAL IMAGE PROCESSING IN WIND ENGINEERING

By

George Wu, Koji Higuchi, and Robert N. Meroney
Colorado State University

Fluid Mechanics and Wind Engineering Program
Department of Civil Engineering
Colorado State University
Fort Collins, Colorado 80523

Prepared for
8th International Conference on Wind Engineering
University of Western Ontario
London, Ontario, CANADA
8-12 July 1991

CEP90-91GW-KH-RNM-12

Applications of digital image processing in wind engineering

G. Wu, K. Higuchi, and R.N. Meroney[a]

[a] Fluid Mechanics and Wind Engineering Program, Civil Engineering Department, Colorado State University, Fort Collins, CO 80523

Abstract

This paper reviews the application of modern digital image analysis and processing techniques to physical modeling of typical wind engineering flow conditions. Using low-cost conventional image capture hardware and software it is possible to measure flow velocities, turbulence characteristics in turbulent shear layers, or, alternatively specify instantaneous and average plume dispersion features.

1. INTRODUCTION

In wind engineering flow visualization traditionally provides guidance to the design of wind tunnel experiments, supports interpretation of local probe measurements, and determines qualitative information concerning the flow phenomena. Any quantitative results extracted with flow visualization techniques have been either so laboriously obtained that only a few data points can be generated or are of limited accuracy, since they are based on subjective manual analysis of the record.

Recently computer technology has provided a new method of making objective automatic analyses of flow visualization images. Through digital image processing technology, one can obtain more temporal and/or spatial information on flow or concentration fields. This information is quite difficult to gather using traditional point-sampling techniques. Use of the digital image processing technology can also provide a connection between wind tunnel and numerical models.

The digital image processing technique is already an important element of wind engineering research. An increasing number of researchers have used this technology to study particle tracking, and concentration measurements. Figure 1 summarizes some of the applications for digital image process methods to wind engineering.

Articles by the Von Karman Institute [1] and Hesselink [2] review digital image processing methods to assist flow visualization. Numerous papers concerning velocity measurements are presented in the Proceedings of the Third and Fourth International Symposia on Flow Visualization and the ASME 1989 winter meeting, Yang [3], Veret [4], and Khalighi [5]. Huber and Arya [6], and Lee *et al.* [7] have used this technology extensively to study dispersion problems in wind tunnel experiments. J.T. Lee et al.[7] used a video image analysis system to measure vertically integrated concentrations in a wind tunnel test.

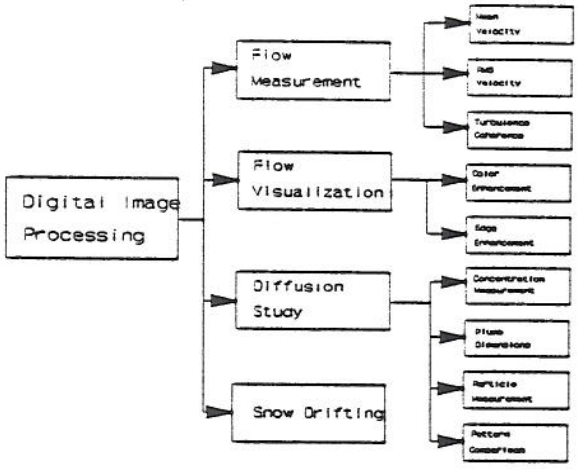

Figure 1. Applications of digital image processing to wind engineering.

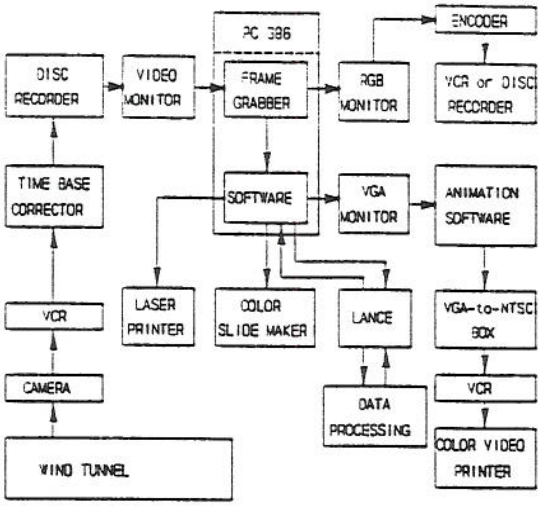

Figure 2. Schematic of Video Image Analysis System (VIPS).

Their results indicated that over a limited range of operating conditions, the video image analysis system can directly measure vertically integrated concentrations. They applied this technology to wind tunnel simulation of dispersion in building wakes. This paper describes a video image analysis system developed in the Fluid Dynamics and Diffusion Laboratory (FDDL) at Colorado State University.

2. VIDEO IMAGE PROCESSING SYSTEM

The hardware components of the Colorado State FDDL Video Image Processing System (VIPS) are shown in Figure 2. The VIPS has four principle elements: an image capturing element, an image digitizing element, an image processing element, and an image presentation element. The image capturing part of the system includes a SVHS camcorder and a four-head, one-half inch tape VCR recorder. Recorded images may be edited into convenient sequences using a dual-monitor, dual-SVHS VCR recorder editing system. Unfortunately, most VCR systems cannot be controlled well enough to maintain adequate picture registration when advancing frame-by-frame under computer control (Lee et al.,[7]). Hence, the edited VCR tape must be additionally recorded onto a video disk. Currently this transfer is being accomplished using the facilities of another laboratory.

Computer control may be used to command a video-disk player to project each individual video frame to a high-resolution video monitor.The key element in the VIPS image digitizing element is a high-resolution image capturing board (DT2853) installed in a PC-386 compatible microcomputer. A standard NTSC video signal (30 frames/sec) can be digitized with 8-bit precision. The board being used produces an intensity field of 512 x 512 pixels at 256 possible gray levels. Given the image interweaving typical of an NTSC video signal the frames can be split to provide images at 60 frames/sec.

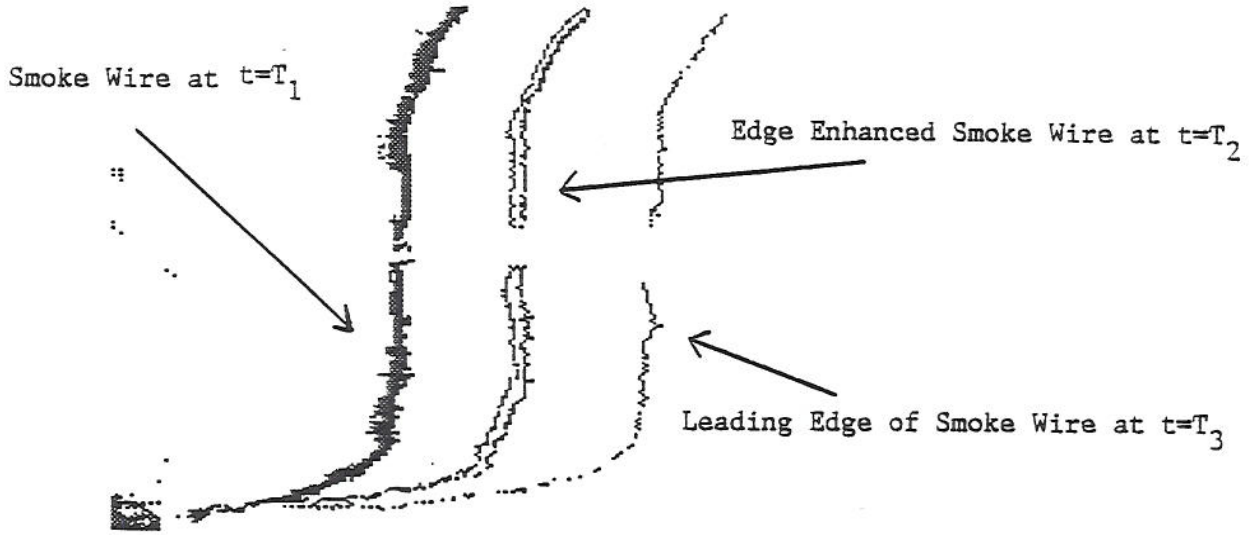

Figure 3. Enhancements of a smoke-wire video image.

operator is

$$R[P(i,j)] = \mathrm{Max}[|P(i,j)-P(i+1,j+1)|,\ |P(i+1,j)-P(i,j+1)|], \tag{1}$$

As soon as the position of the smoke line is determined the image is made uniformly bright by using a thresholding algorithm such as

$$B[P(i,j)] = \begin{matrix} 1 \text{ if } R[P(i,j)] > T \\ 0 \text{ if } R[P(i,j)] < T' \end{matrix} \tag{2}$$

where T is the threshold which defines the edge. Figure 3 presents a example for this process. A coordinate image taken in the same plane as the smoke pathlines can then be superimposed on the smoke wire realization to improve the registration of coordinate locations.

During data reduction a software program calculates local velocities from the new image data base. Two vertical sample lines, SL_1 and SL_2, may be designated in space downwind of the nichrome wire. The data base is then searched for the times, T_1 and T_2, that the pixel locations are turned on. Given $dX = X_{SL1} - X_{SL2}$, and $dT(x,y) = T_2(x+dx,y) - T_1(x,y)$, then the local velocity $U(x,y,t) = dX/dT$. Similar manipulations may provide values for local vertical velocities, $W(x,y,t)$.

Since many thousands of images may be obtained from a short TV tape record, it is possible to define average velocities as

$$U_{mean}(x,y) = \Sigma U_i(x,y,t)/N, \tag{3}$$

and the turbulence intensities as

The VIPS image processing element is based on a commercial subroutine library developed by DATA TRANSLATION. The size of a typical video image is about 263 Kbyte, which is too big to allow the manipulation of two images simultaneously in an MS-DOS operating system. Therefore an IBM Operating System/2 (OS/2) is used for program development. Through the VIPS image processing element the video image may be processed by: a) subtracting the background, b) overlaying a coordinate system, c) enhancing front, center, or back edge of the image, or d) assigning colors to different grey intensity levels. As noted in the following sections one can also extract edge pixel locations to calculate velocities, plume parameters or combine images to provide animation.

The VIPS image presentation element includes hardware to project the image to a RGB or VGA monitor; store the digital image on floppy or hard disks, streaming tapes, optical digital disk, or on network file-servers. It also allows the digitized image to be printed on a laser printer or color slide maker. Alternatively, a VGA-to-NTSC hardware card can reformulate the signal to record the enhanced image on a conventional VCR or a color video printer.

3. PROCESSING OF SMOKE WIRE IMAGES

Low-speed velocity measurements made in thermally stratified flows are often difficult to collect using conventional techniques of measurement. Pressure type devices like pitot-static tubes are not adequately sensitive at speeds below 1 m/sec; hot-film and pulsed-wire anemometry results are difficult to interpret, and even expensive laser-doppler velocimeters require extra Bragg cell components and optical traversing equipment.

A smoke-wire method has been used at Colorado State in the past to evaluate the characteristics of low-speed thermally-stratified shear flows (Yamada [8], Orgill [9]). In the smoke-wire method, oil is vaporized from a very thin, high-resistance nichrome wire by heating it with a high-voltage electric pulse. A thin line of oil vapor smoke is formed and transported downwind by the local flow field in the wind tunnel. After a timed delay, a strobe light illuminates the smoke line to record its behavior on photographic film. Photogrametry techniques are then used to calculate the smoke displacement, which is combined with the known time delay to specify the velocity field. Stereo-camera arrangements permit determination of all three velocity components. The accuracy of the velocity field is limited by inertia and buoyancy of the smoke vapor, photogrametric measurement reliability, and the limited number of realizations evaluated.

Digital image processing and image enhancement methods now provide a means to modernize and significantly improve the conventional smoke wire technique. The visible behavior of the smoke line is now recorded on a high-resolution television camera system on VCR tape. The analog images may be transformed into digital arrays, and the images can then be enhanced and manipulated by a computer system.

As noted above processing of the smoke wire images requires data acquisition followed by data reduction. Each smoke wire image is digitized and sequentially stored together with its time index in a data base. The image is digitized from left to right, top to bottom yielding a two-dimensional array of image pixels and intensities, P(i,j).

During data acquisition the digitized image is subtracted from a background image and the position of the smoke line enhanced by edge detection. Robert's edge detection operator described by Gonzales and Wintz [10] was chosen to produce a single bright line. Robert's

$$\overline{u^2}(x,y) = \Sigma \left([U(x,y,t) - U_{mean}(x,y)]^2, \right. \quad (4)$$

To validate hardware and software techniques described above simultaneous hot-film and smoke-wire measurements were made in a turbulent boundary layer. Measurements were collected in the Meteorological Wind Tunnel (MWT) of the FDDL. A boundary layer was developed over a rough floor at a wind speed of 0.5 m/s. The flow produced a boundary layer 0.35 meters deep with a power law index, α, equal to 0.21. Figure 4 presents a comparison between the two sets of measurements. One-thousand images of the smoke line were examined to create the average velocity and turbulent intensity profiles. Mean velocity and longitudinal turbulence profiles were identical within the statistical variability of the hot-film measurements.

4. PROCESSING OF SMOKE PLUME IMAGES

A wind tunnel experiment was performed to demonstrate an application of the digital image processing to dispersion. Video image and gas chromatograph (GC) measurements were made of a plume emitted from a model stack height. Figure 5 presents the general configuration of the experiment.

A mixture of propane and nitrogen gas was released from the stack to provide a detectable plume for concentration measurements. A smoke generator was used to generate a visible plume for image analysis. Figures 6 and 7 show an instantaneous plume image and a time averaged plume image. The instantaneous plume image is one video frame (1/30 second interval). The instantaneous plume image illustrates the turbulent nature of the flow. The time averaged plume image is the ensemble average of 5,000 video frames (an averaging

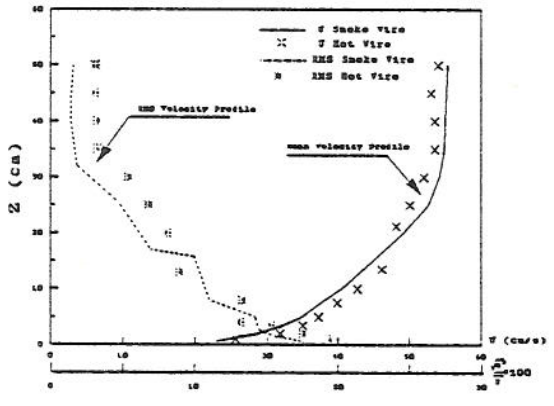

Figure 4. Boundary-layer profiles of mean velocity and turbulence measured by hot-film anemometry and video image analysis.

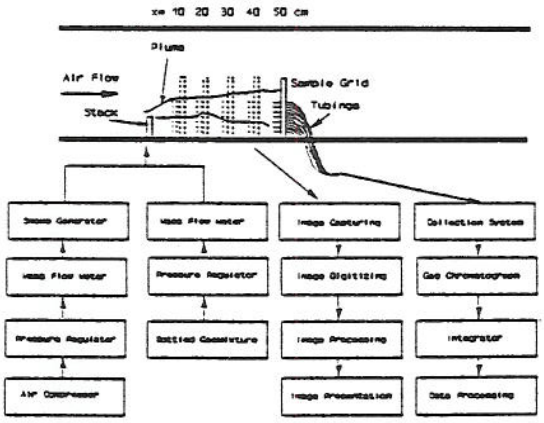

Figure 5. Schematic of scalar transport experiment in wind tunnel-image analysis system and gas chromatograph system.

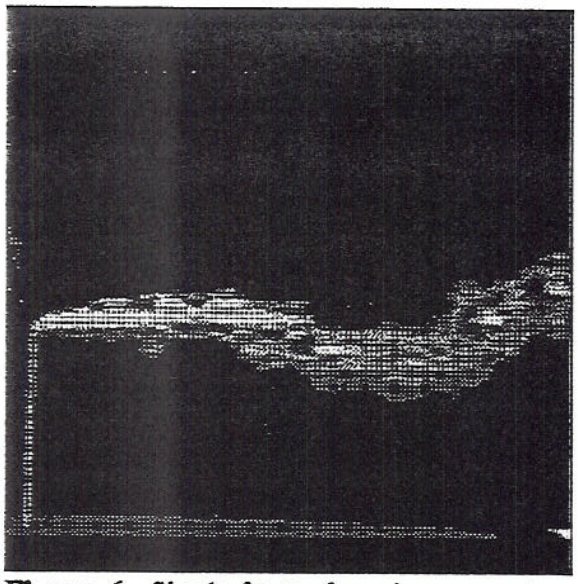

Figure 6. Single frame from image capture system. Images taken a 1/30 sec intervals.

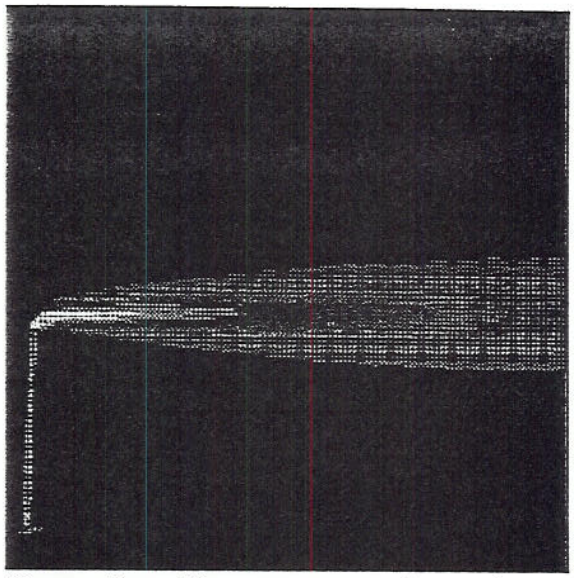

Figure 7. Time average plume image based on the ensemble of 5000 instantaneous frames.

period of about 167 seconds). From the time averaged plume image it could be confirmed that the distribution of plume intensity was Gaussian in nature. i.e.

$$I = I_{max} / (\sqrt{2\pi} * \sigma_z) * e^{-(z-z_{max})^2/(2*\sigma_z^2)}, \quad (5)$$

where I_{max} is a maximum intensity and z_{max} is the coordinate of the maximum intensity. Figure 8 displays the digitized video image intensity data for a time averaged plume at x = 10, 20, 30, 40 and 50 cm from the stack compared to Gaussian distributions.

Other plume parameters such as plume width σ, plume rise, and peak-to-mean ratio may also be measured using digital image processing techniques. The position of the plume centerline is an important parameter for studying plume rise, plume downwash, and the location of maximum pollutant concentrations downwind of obstacles. Traditionally, plume location is determined by visual examination of photographs (Peterson [11]). This method is quite subjective and time consuming. Alternatively, VIPS technology locates the plume center line as the downwind locus of the maximum pixel intensities

Many numerical dispersion models are based on the Gaussian model which require estimates

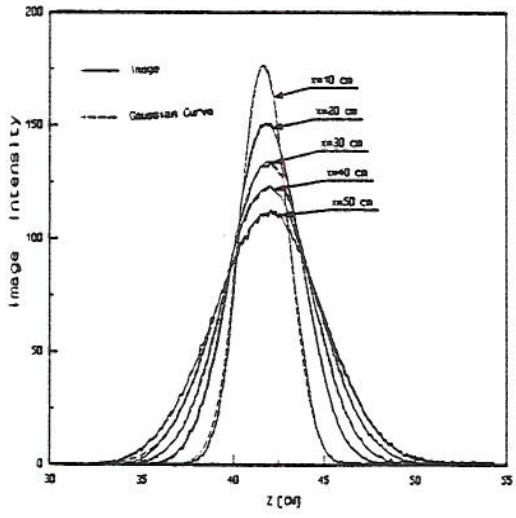

Figure 8. Lateral plume growth as depicted by image intensity variations at various downwind distances from source.

of plume growth, σ_y and σ_z. Most published σ_y and σ_z curves are based on field experiments performed during the 1950's and 1960's. Wind tunnel specification of σ_y and σ_z are usually based on GC concentration measurement data. Sample measurement density and instrument time response limit the number of such measurements.

Gifford [12] developed an expression for plume width, σ_y, which can be derived from a plume photograph. He assumed that the time average plume has a Gaussian distribution. Then dispersion parameters σ_y and σ_z are functions of the visible edge of the plume where σ_y can be expressed as

$$\sigma_y^2(x) = Y_E^2/\ln(e*Y_M^2/\sigma_y^2), \tag{6}$$

where x is the downwind distance of the stack position, Y_E is the half-width of the plume at downwind distance x from the source, Y_M is the maximum half-width of the plume, and e is the base of natural logarithms.

Alternatively, Pasquill [13] proposed a new equation in which plume height, σ_z, appears raised to an arbitrary power, s, where

$$\sigma_z^s(x) = s*\gamma^{s/2}*Z_E^s/[\ln(e*Z_M^s/\sigma_z^s) - s/2*\ln(s*\gamma)], \tag{7}$$

where Z_E is the height of the visible plume edge and Z_M is the maximum value of Z_E and

$$\gamma = \Gamma(3/s)/\Gamma(1/s), \tag{8}$$

where Γ is the gamma function. For s = 2, this equation reduces to Equation (6) Nappo [14] and other researchers have used these equations to calculate σ_y and σ_z by manually measuring plume dimensions Y_E, Z_E, Y_M, and Z_M from plume photographs.

These equations were incorporated into the image processing program. Standard deviations, σ_y and σ_z, are calculated as soon as the plume image is digitized from the VIPS. Procedures to obtain the plume centerline, Z_c, and the dispersion parameter , σ, from the video image data are described below.

1) Subtract a background image from a time averaged plume image,
2) Find the edge of a plume and maximum gray level points,
3) Set the maximum gray points to the plume centerline, and
4) Use one of three methods to obtain the dispersion parameter, σ,

Method a)

$$\sigma_z^s(x) = s*\gamma^{s/2}*Z_E^s/[\ln(e*Z_M^s/\sigma_z^s) - s/2*\ln(s*\gamma)], \tag{9}$$

where s=2, or

Method b)

$$\sigma_z^2 = \Sigma z_i^2 I_i / \Sigma I_i, \tag{10}$$

where z_i is the z-axis coordinate from the centerline and I_i is a video image intensity, or

Method c) The distributions of the plume image intensity are assumed Gaussian. Therefore, σ_y and σ_z are calculated by a curve fitting program based on Equation 5.

Figures 9 and 10 record the measured plume rise, Z_c, and plume-width, σ_z, respectively. An empirical plume centerline expression recommended by Briggs is plotted in Figure 10 as a solid line, where

$$z_c/l_m = (3/\beta_m^2)^{1/3} * (x/l_m)^{1/3} = C_m * (x/l_m)^{1/3}, \quad (11)$$

in which x is a downwind distance of a stack position, z_c' is the rise of plume centerline above the stack, β_m is the entrainment coefficient for jets, C_m is a related constant, and l_m is a momentum length scale defined as

$$l_m = F_m^{1/2}/U = (\rho_s/\rho_a)^{1/2} * D * W_s/2U, \quad (12)$$

where U is the ambient air speed, W_s is the stack effluent exit speed, D is the internal stack diameter, and ρ_a and ρ_s are the density of the ambient air and the stack effluent respectively. From Figures 9 and 10 we observe that the plume centerline moves slightly upward near the stack due to the stack effluent momentum. The σ_z increase linearly with downwind distance.

Peak-to-mean ratio concentration ratio characterizes plume concentration fluctuations. Gifford [15] proposed a formula to calculate the peak-to-mean ratio for a source at height H_s,

$$P/M(x,y,z) = (\sigma^2+D^2)/\sigma^2 * \exp[y^2/(2(\sigma^2+D^2) + (z-H_s)^2/(2(\sigma^2+D^2)], \quad (13)$$

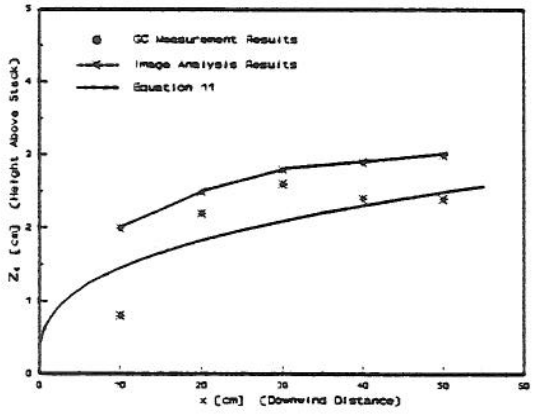

Figure 9. Centerline of plume measured by image intensities and gas chromatograph analysis.

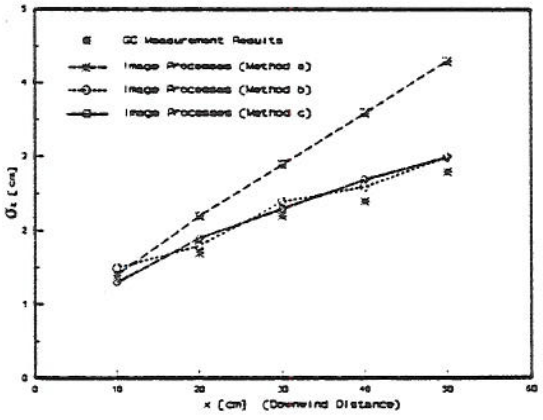

Figure 10. Vertical plume growth measured by image and gas chromatograph analysis.

where it is assumed that $\sigma_y = \sigma_z = \sigma$. Air pollution measurements reported by Gifford [15] show that values of P/M are in the range from 2 to 5 for source and receptor at same elevation. Two methods have been used to calculate peak-to-mean ratio using video images,

a) Calculate P/M from Equation 13 using magnitudes of σ^2 and D^2 determined from 1,000 instantaneous plume images, and

b) Calculate P/M directly from the ratio of the instantaneous plume image intensities and the averaged plume image intensity,

$$P/M(x,z) = I_{peak}(x,z)/I_{mean}(x,z), \tag{14}$$

where $I_{peak}(x,z)$ is maximum video image intensity on the z-axis and $I_{mean}(x,z)$ is the corresponding mean intensity of a time averaged plume image. One thousand instantaneous plume images were also used to do ensemble averaging.

Figures 11 and 12 show the P/M ratio at x = 10, 20, 30, 40, and 50 cm downwind from the stack obtained by using methods a) and b), respectively. Note that the P/M ratio in Figure 11 is at (x,0,z) but that in Figure 12 is at (x,z), i.e. which is horizontally integrated. The P/M ratios in these figures near $(z-h_s)/\sigma_z = 0$ are between 2 to 5, which agrees with Gifford (1960)'s statement. The five curves in each figure are very close to a single curve similarity exists based on plume width.

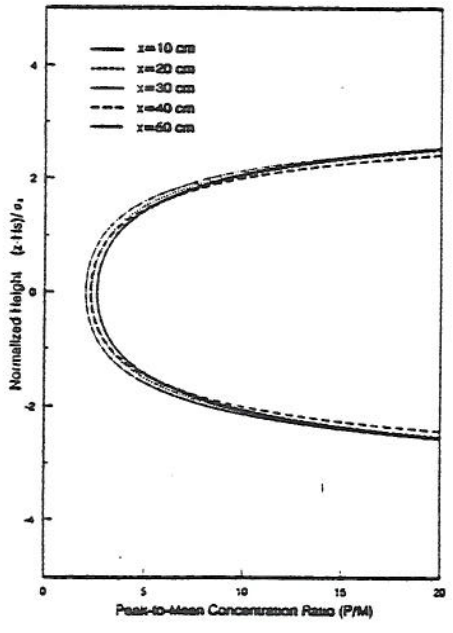

Figure 11. Peak-to-mean concentration ratio calculated from measured plume displacement and widths using Equation 13.

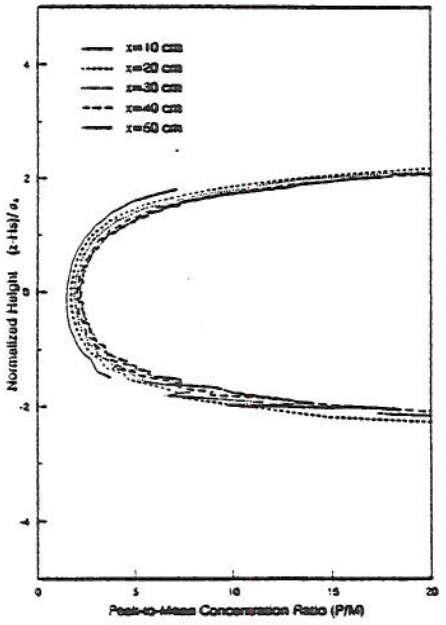

Figure 12. Peak-to-mean ratio calculated directly from measured instantaneous and average values of pixel intensity.

5. CONNECTION BETWEEN WIND TUNNEL AND NUMERICAL MODELS

Digital image processing can also provide an interpretive connection between wind tunnel and numerical models. Statistical data can be obtained directly from the deformation, concentration, and relative motion of visual media in the wind tunnel. Yet the behavior of flow can also be predicted using large, multidimensional computational fluid dynamic programs. Figure 13 presents a schematic of the processes required to produce visual comparison of fluid and numerical modeled flows. In the example shown in Figure 14 the top picture is produced by a 5000 frame ensemble average plume image of a wind tunnel experiment. The bottom plume is produced numerically from a Gaussian dispersion plume model.

6. CONCLUSIONS

This paper has reviewed application of video image analysis techniques and digital image processing methods to wind engineering. From the examples considered we found that accurate flow field and scalar transport measurements may be produced. Current research is directed toward developing reliable methods to produce quantitatively useful concentration measurements through image analysis and processing.

7. ACKNOWLEDGEMENTS

Fiscal support through National Science Foundation Cooperative Agreement BCS-9045652 and Office of Naval Research Grant N00014-88-K-0029 A00001 is gratefully acknowledged. Advice and support from Dr. Elenora Sabaddell, NSF, and Dr. Robert Abbey, ONR, Dr. J.T. Lee, Los Alamos National Laboratory, are appreciated.

8. REFERENCES

1 Von Karman Institute, "Digital Image Processing in Fluid Dynamics" Lecture Series 1984-03, Von Karman Institute for Fluid Dynamics, Belgium (1984).
2 Hesselink,L., "Digital Image Processing in Flow Visualization" Ann. Rev. Fluid Mech. Volume 20 (1988) 421-485.
3 Yang,W.J., "Flow Visualization III", Proceedings of Third International Symposium on Flow Visualization, Ann Arbor, Michigan, Hemisphere Publishing Corp., New York, NY. (1985)
4 Veret,C., "Flow Visualization IV", Proceedings of the Fourth Internal Symposium on Flow Visualization, Paris, France, Hemisphere Publishing Corp., New York, NY (1987).
5 Khalighi, B.,"Flow Visualization-1989", Proceeding of the ASME the Winter Annual Meeting, San Francisco, CA (1989).
6 Huber, A.H., and Arya, S.P., "Video Images of Smoke Dispersion in the Near Wake of a Model Building", J. Wind Engr. Ind. Aerodyn., 32 (1989) 263-284.
7 Lee, J.T., Call, D.L., Lawson, R.E. Jr, Clements, W.E., and Hoard,D.E., "A Video Image Analysis System For Concentration Measurements and Flow Visualization in Building Wakes", Los Alamos National Laboratory Report No. LA-UR-88_3853, (1988)

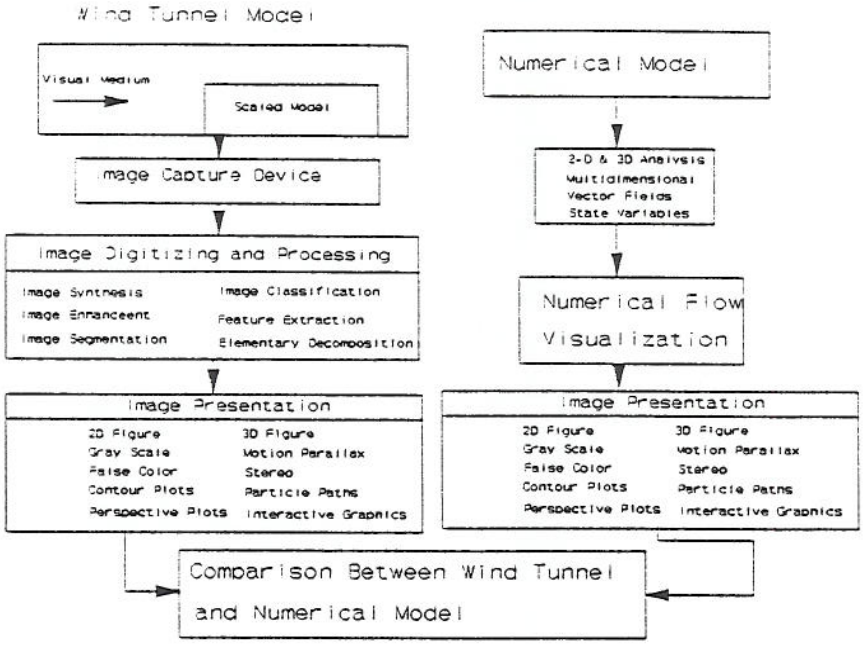

Figure 13. Schematic of comparison processes between empirical image analysis and numerical calculations.

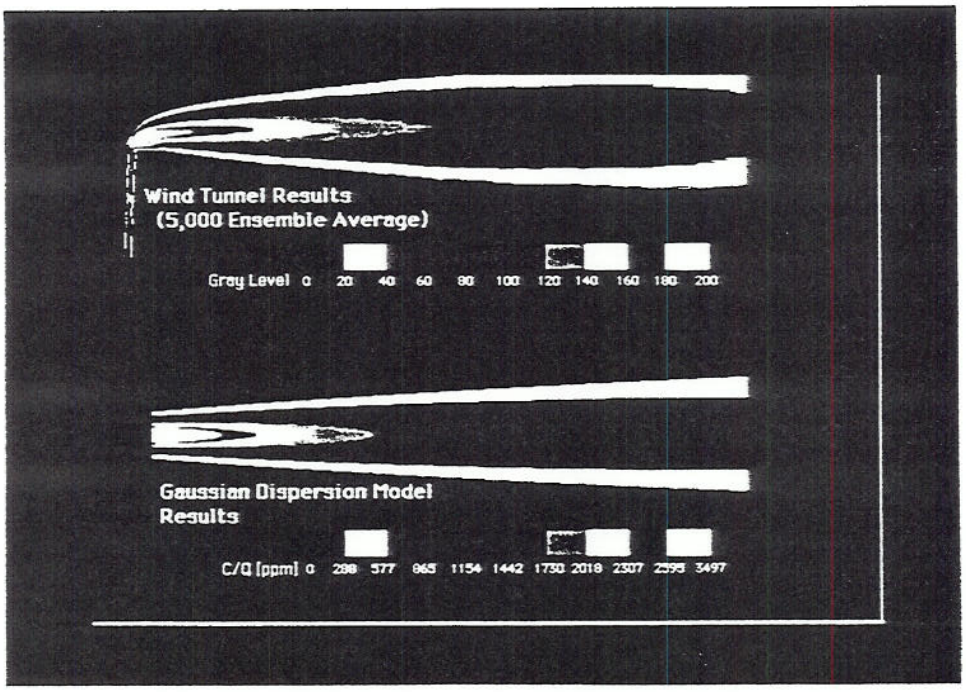

Figure 14. Grey scale images of concentration contours produced by image analysis compared with numerical calculations.

8 Yamada, T. and Meroney, R. N., "Numerical and Wind Tunnel Simulation of Response of Stratified Shear Layer to Nonhomogeneous Surface Features" Final Report, CER70-71TY-RNM62, Colorado State University (1971).
9 Orgill, M.M., "Laboratory Simulation and Field Estimates of Atmospheric Transport-Dispersion Over Mountainous Terrain" PhD Dissertation. CED70-71MMO27, Colorado State University (1971).
10 Gonzales, R.C., and Wintz, P., "Digital Image Processing", Addison-Wesely, Reading, Massachusetts (1988).
11 Petersen,R.L. , "Plume Rise and Dispersion for Varying Ambient Turbulence, Thermal Stratification and Stack Exit Conditions", PhD Dissertation. CED78-79RLP22, Colorado State University (1978).
12 Gifford, F.A., "Smoke Plumes as Quantitative Air Pollution Indices", Int. J. of Air Poll., 2 (1959) 42-50.
13 Pasquill, F., "Atmospheric Diffusion", John Wiley, New York (1974).
14 Nappo, C.J., "Turbulence and Dispersion Parameters Derived from Smoke-Plume Photoanalysis", Atmos. Environ., 18 (1984) 299-306.
15 Gifford, F.A., "Peak to Average Concentration Ratios According to Fluctuating Plume Dispersion Model", Int. J. of Air Poll., 4 (1960) 253-260.